JOC The Journal of Organic Chemistry

Article

pubs.acs.org/joc

Preparation and Spectroscopic, Magnetic, and Electrochemical Studies of Mono-/Biradical TEMPO Derivatives

Miroslav Kavala,[†] Roman Boča,[‡] Lubomír Dlháň,[‡] Vlasta Brezová,[§] Martin Breza,[§] Jozef Kožíšek,[§] Marek Fronc,[§] Peter Herich,[§] Lubomír Švorc,[∥] and Peter Szolcsányi*[,†]

[†]Department of Organic Chemistry, [‡]Department of Inorganic Chemistry, [§]Department of Physical Chemistry, and [∥]Department of Analytical Chemistry, Faculty of Chemical and Food Technology, Slovak University of Technology in Bratislava, Radlinského 9, SK-812 37 Bratislava, Slovakia

Supporting Information

ABSTRACT: A comparison set of mono-/biradical TEMPO derivatives was prepared, novel compounds were fully characterized, and their physicochemical properties were determined. Cyclic voltammetry revealed reversible redox behavior for all studied nitroxides. Moreover, the electron-withdrawing substituents increased the oxidation potential of the respective nitroxides in comparison to electron-donating groups. While EPR spectra of monoradicals in dichloromethane at 295 K reveal the expected three-line signal, spectra of biradicals show more complex features. DFT and MP2 calculations indicate that the EPR splitting pattern of dinitroxide **7** could be explained by its interactions with solvent molecules. In the solid state, mononitroxides **4** and **5** behave as a Heisenberg antiferromagnetic chain, whereas dinitroxides **6**−**8** are almost isolated paramagnetic diradicals coupled in an antiferromagnetic manner.

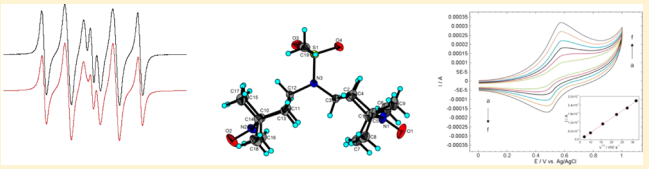

INTRODUCTION

Nitroxides as stable organic radicals[1] represent an interesting class of molecules that form the basis of novel and/or emerging functional materials as radical batteries,[2] spin probes,[3] polarizing agents for DNP-NMR,[4,5] antioxidants,[6] magneto-active materials,[7] and radiation protective agents.[8] Arguably, the most prominent representative of nitroxide-type radicals is TEMPO (2,2,6,6-tetramethylpiperidine-*N*-oxyl).[9,10] Its 4-oxo derivative **1** (oxo-TEMPO) is used as a polymerization catalyst,[11] the 4-hydroxy derivative **2** (TEMPOL) shows antihypertensive effects,[12] and 4-amino-TEMPO **3** (Figure 1) was recently identified as a new target for neuro-drug discovery.[13] From a methodological point of view, not only are compounds **1**−**3** useful oxidants in organic synthesis[14] but they also serve as optimal substrates for the preparation of novel nitroxide analogues.

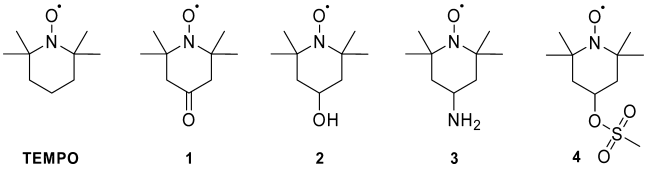

Figure 1. TEMPO and its known C(4)-heteroatom-substituted derivatives **1**−**4**.

Thus, we have prepared the known monoradical[15] **5** and biradical[16] **7**, as well as novel biradicals **6** and **8** bearing the TEMPO moiety (Figure 2), and investigated their structural influence on the spectroscopic, magnetic, and electrochemical properties.

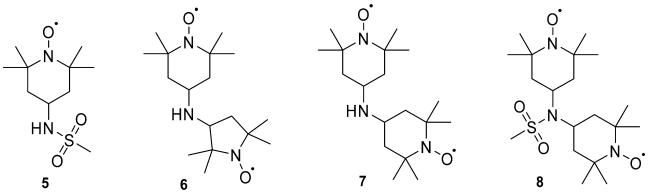

Figure 2. Mono-/biradical TEMPO derivatives **5**−**8** used in this study.

RESULTS AND DISCUSSION

Synthesis. While TEMPO and its derivatives **1**−**4** are commercially available, nitroxides **5**−**8** were prepared by standard synthetic protocols. Thus, the sulfonamide **5** was accessed by a two-step procedure starting from 4-amino-2,2,6,6-tetramethylpiperidine via its quantitative mesylation and subsequent oxidation of the hydrochloride salt **9** in 85% overall yield (Scheme 1).

Next, biradicals **6** and **7** were prepared by reductive amination[17] of oxo-TEMPO **1** with amino-PROXYL **10** (for **6**: 46%) or with 4-amino-TEMPO **3** (for **7**: 64%) using sodium cyanoborohydride in acidic methanol under nonoptimized reaction conditions (Scheme 2). The following mesylation of biradical **7** toward the sulfonamide **8** proved to be unexpectedly

Received: April 23, 2013

   dx.doi.org/10.1021/jo400845m | *J. Org. Chem.* XXXX, XXX, XXX−XXX

Scheme 1. Preparation of Nitroxide 5

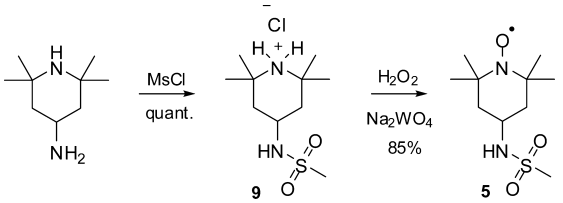

difficult. While the use of excess of methanesulfonyl chloride in combination with various bases (triethylamine, *N*,*N*-diisopropylethylamine, 1,8-diazabicyclo[5.4.0]undec-7-ene, imidazole, 1,8-bis(dimethylamino)naphthalene, sodium hydroxide, and potassium carbonate) in various solvents (dichloromethane, 1,4-dioxane, toluene, and diethyl ether) afforded **8** up to only 15% yield, the use of a 5-fold molar excess of methanesulfonyl anhydride delivered the desired sulfonamide **8** in 35% yield (Scheme 2).

With the desired mono-/biradicals **5**–**8** in hand, we investigated their spectroscopic (EPR), magnetic (SQUID), and electrochemical (CV) properties. We have also performed single-crystal X-ray analyses of compounds **4**–**8** and elucidated their solid state structures.

Cyclic Voltammetry. The redox potentials of the nitroxides **1**, **2**, and **4**–**8** were determined by cyclic voltammetry (CV) in phosphate buffer solution (PBS, pH 7.0), using a paraffin-impregnated graphite electrode (PIGE). In general, stable cyclic nitroxides undergo one-electron oxidation, reflecting the formation of the corresponding *N*-oxoammonium cations.[18] Cyclic voltammograms of **1**, **2**, and **4**–**8** reveal that all of the studied compounds undergo a one-electron transfer process with half-wave potentials ($E_{1/2}$) in the range of 401−616 mV vs Ag/AgCl electrode (Table 1). In all cases except for **1**, the anodic and cathodic peak currents are approximately equal, and thus it may be concluded that nitroxides **2** and **4**–**8** are reversibly oxidized to their corresponding *N*-oxoammonium cations (Figures S9–S13 in the Supporting Information). However, the intensities of the anodic and cathodic currents were far from equal for oxo-TEMPO **1**, indicating a loss of the kinetic reversibility[19] (Figure S8 in Supporting Information). On the other hand and in comparison, the half-wave potential ($E_{1/2}$) values of TEMPO and mononitroxide **2** corresponded well with those previously reported.[20−22] Due to the different

Table 1. Experimental Redox Potentials and Current Responses of Nitroxide/*N*-Oxoammonium Cation Redox Couples[a]

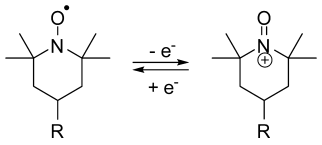

nitroxide	E_{pa} (mV)	E_{pc} (mV)	$E_{1/2}$ (mV)	ΔE (mV)	i_{pa}/i_{pc}
TEMPO	462	340	401	122	1.1
1	614	520	616	94	4.5
2	538	410	474	128	1.1
4	600	494	547	106	1.1
5	558	450	504	108	1.2
6	549	449	499	100	1.2
7	574	466	520	108	1.2
8	644	490	567	154	1.1

[a]Definitions: E_{pa} = anodic peak potential, E_{pc} = cathodic peak potential, $E_{1/2} = (E_{pa} + E_{pc})/2$, $\Delta E = E_{pa} - E_{pc}$, i_{pa} = anodic peak current, i_{pc} = cathodic peak current.

natures of the carbonaceous electrode surfaces used (PIGE vs GCE), there is an almost constant increment of potential, being approximately 130 mV for both nitroxides TEMPO (401 vs 522 mV) and **2** (474 vs 611 mV).

The experimentally determined values of redox potentials of nitroxides **1**, **2**, and **4**–**8** are summarized in Table 1.

The results indicate an emerging trend that the electron-withdrawing substituents (OMs, HNMs) tend to increase the oxidation potential of a nitroxide in comparison to electron-donating groups (OH, NH_2; cf **2** vs **1** and **4** and **7** vs **8**; Figure 3). Thus, our empirical observations verify the recently postulated influence of the nature of ring substituents on the one-electron-oxidation potential of cyclic nitroxide radicals.[23] Interestingly, the shapes of cyclic voltammograms of mono-nitroxides **1**, **2**, **4**, and **5** and dinitroxides **6**–**8** are analogous throughout the series (Figures S5–S13 in Supporting Information), thus indicating that electrochemical oxidation of biradicals **6**–**8** likely involves simultaneous one-electron transfer to both radical centers rather than a stepwise process.

In addition, we have observed a noteworthy anodic potential of biradical **8** (E_{pa} = 644 mV) that is higher than the corresponding value for 4-oxo-TEMPO **1** (E_{pa} = 614 mV). The

Scheme 2. Preparation of Dinitroxides 6–8

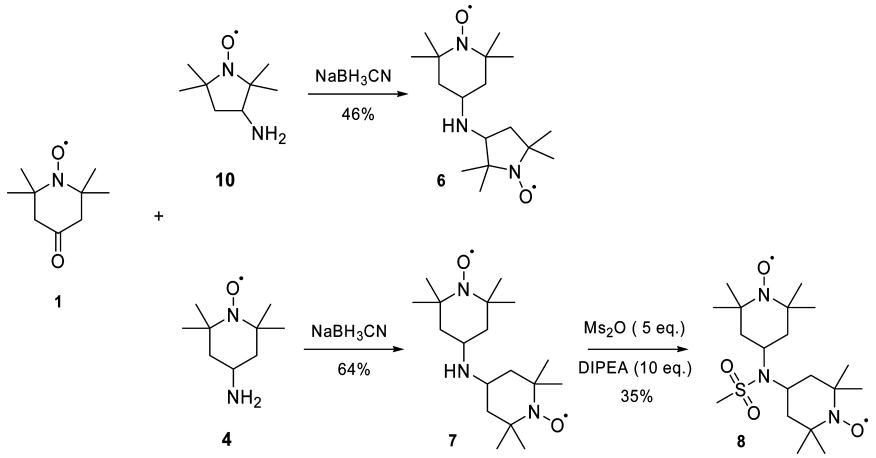

dx.doi.org/10.1021/jo400845m | J. Org. Chem. XXXX, XXX, XXX–XXX

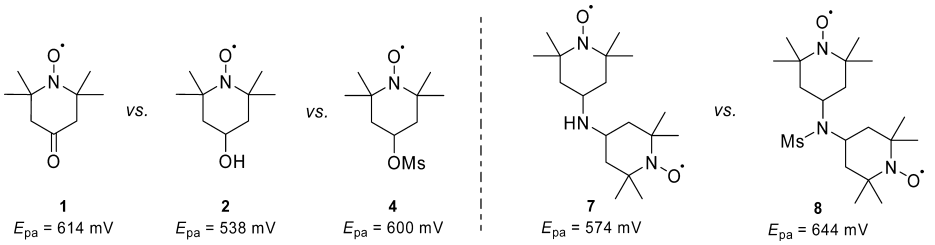

Figure 3. Comparison of ring substituent influence on the oxidation potential of nitroxides.

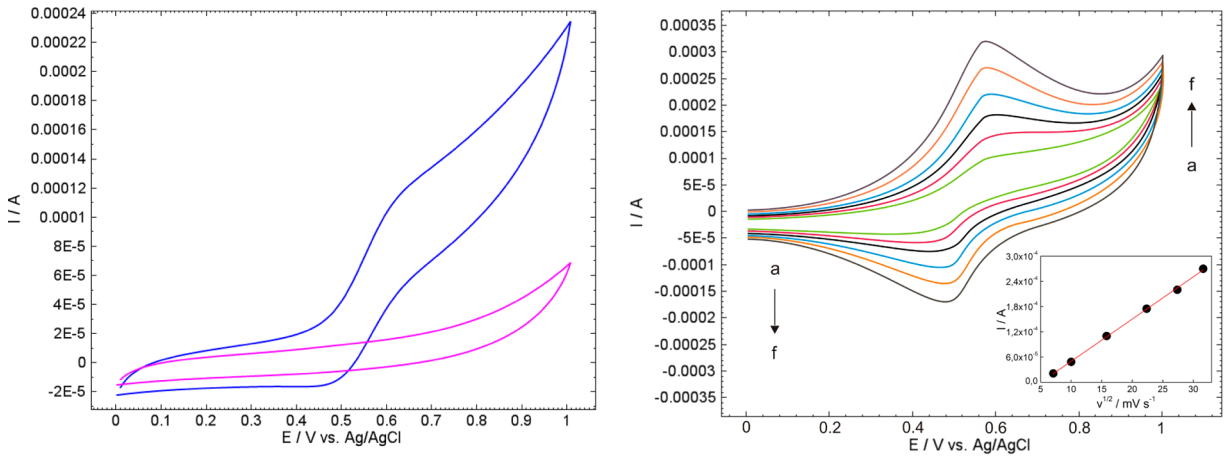

Figure 4. (left) Cyclic voltammogram of the nitroxide/*N*-oxoammonium couple of **8** (blue) vs control (pink): scan rate 100 mV s^{-1}, concentration 1 × 10^{-4} mol L^{-1} in PBS at pH 7.0 on a PIGE electrode. (right) Influence of scan rate on current response in the CV of biradical **8**: concentration 1 × 10^{-4} mol L^{-1} in PBS at pH 7.0 on a PIGE electrode. Scan rates: (a) 50, (b) 100, (c) 250, (d) 500, (e) 750, and (f) 1000 mV s^{-1}. Inset: dependence of anodic peak current on the square root of the scan rate.

peak separation values are higher (ΔE = 94−128 mV) in comparison to the theoretical Nernstian value (59 mV); however, the electrode reactions of the studied nitroxides are considered to be kinetically reversible. Moreover, biradical **8** provides the largest separation of respective redox potentials (ΔE = 154 mV; Figure 4).

Useful information on the mechanism of the electrode process (rate-determining step) can be obtained from the relationship between the peak current and scan rate (v). As an illustrative example, Figure 4 displays the effect of scan rate on the current response of biradical **8** within the range 50−1000 mV s^{-1}. It was found that the oxidation (inset of Figure 4) and reduction currents of biradical **8** increased linearly with the square root of scan rate. This dependence of the oxidation process can be expressed by eq 1:

$$I(\mathrm{A}) = -[8.056(\pm 0.102)] \times 10^{-7} + [1.012(\pm 0.014)] \times 10^{-5} v^{1/2}\ \mathrm{mV\ s^{-1}} \quad R^2 = 0.998 \qquad (1)$$

The high linearity and low intercept value suggest that diffusion is the rate-determining step in the electrode process of biradical **8** and that the rate-limiting adsorption and/or specific interactions on the PIGE electrode are thus negligible. A similar phenomenon was also observed in the case of all other studied nitroxides **1**−**7**.

EPR Spectroscopy and DFT Calculations. The room-temperature X-band EPR spectra of mononitroxides **1**, **2**, **4**, and **5** in DCM revealed a three-line signal corresponding to the dominant hyperfine coupling of unpaired electron with the nitrogen nucleus (Figure S14 in the Supporting Information). Further analyzed hyperfine coupling constants (Hfcc) were attributed to the hydrogen nuclei of two equatorial and two axial methyl groups, along with equatorial and axial ring hydrogens (Table 2). In contrast, these interactions are negligible in the EPR spectra[24] of oxo-TEMPO **1** and, moreover, ^{13}C satellites are visible here (Table 2).

EPR spectra of dinitroxides **6**−**8** were analyzed by applying an exchange-coupled spin Hamiltonian, where exchange coupling between two electrons is defined via the exchange coupling constant J.[4,17,25−29] Figure 5 illustrates the EPR spectrum of derivative **6** in DCM, representing a five-line signal characteristic for dinitroxide structures with J values significantly higher than the nitrogen nuclei hyperfine coupling constant ($J \gg A_N$). The derivative **6** possesses two different nitroxide moieties, in good agreement with the nonequivalent nitrogen splittings elucidated from the simulated spectra (A_{N1} = 1.592 mT and A_{N2} = 1.460 mT); simultaneously, small differences in g values were found (Table 2). Surprisingly, similar results were obtained for dinitroxide **7** in DCM, as the simulation analysis of experimental EPR spectra (Figure 5) revealed an asymmetry of nitroxide groups with A_{N1} = 1.528 mT and A_{N2} = 1.640 mT (Table 2). However, nearly equivalent values of A_{N1} and A_{N2} were obtained from EPR spectra of dinitroxide **7** in the nonpolar solvent *n*-heptane (A_{N1} = 1.501 mT and A_{N2} = 1.548 mT). Such an observation raises the question whether this asymmetry resulted from different dinitroxide conformations or from the interactions of particular nitroxide moieties with the solvent molecules (see below).

The EPR spectrum of dinitroxide **8** is more complex (Figure 5), demonstrating a restriction in the exchange coupling ($J > A_N$), and the best simulation fit was obtained using $J \approx 13$ mT (Table 2). In comparison to **7**, the presence of a sulfonamide

dx.doi.org/10.1021/jo400845m | J. Org. Chem. XXXX, XXX, XXX−XXX

Table 2. Spin Hamiltonian Parameters Elucidated from the Simulation of Experimental EPR Spectra of Mono-/Dinitroxide Derivatives 1, 2, and 4−8 Measured in Dichloromethane at 295 K

	hyperfine coupling constant (mT)			
nitroxide	A_{NO}	A	g	exchange coupling constant (cm^{-1})
1	1.484	0.544 (^{13}C), 0.554 (^{13}C)	2.0061	
		0.520 (^{13}C), 0.543 (^{13}C)		
		0.574 (^{13}C), 0.535 (^{13}C)		
2	1.581	0.045 (6H), 0.033 (6H)	2.0062	
		0.039 (2H), 0.001 (2H)		
4	1.571	0.043 (6H), 0.032 (6H)	2.0063	
		0.035 (2H), 0.004 (2H)		
5	1.578	0.052 (6H), 0.037 (6H)	2.0060	
		0.017 (2H), 0.003 (2H)		
6	1.592		2.0064	~0.024
	1.460		2.0061	
7	1.528		2.0065	~0.065
	1.640		2.0063	
8	1.623		2.0065	~0.012
	1.536		2.0063	

spacer in **8** has a noticeable effect on the exchange between two nitroxide units, as summarized in Table 2.

Next, DFT calculations were performed with the aim of obtaining detailed information about the origin of the asymmetry of EPR spectra of **7** in dichloromethane solutions. In the first step, we have varied the mutual orientations of both piperidine rings in **7** with chair conformations of both rings (according to N1−C4 axes) with equatorial N−O bonds. Three stable conformations of this type (characterized by H4−C4−C4′−H4′ dihedral angles in Table 3) have been found by the geometry optimization of **7** in triplet (spin multiplicity $M_S = 3$) and "broken-symmetry" singlet ($M_S = 1$) spin states in vacuum as well as in dichloromethane and *n*-heptane solutions using a CPCM treatment. As there are only vanishing differences between both spin states (except different signs for spin densities), only data for the triplet spin state are presented. As can be seen from Table 3, N−O spin densities (as well as the corresponding A_N values) do not depend on mutual ring orientations. This might be a consequence of no spin density at the central amine nitrogen. Energy data indicate that at room temperature only two conformers (**7a**,**b**) are present in relevant concentrations and their relative abundance depends on the solvent used. Nevertheless, N−O spin densities and A_N values practically do not depend on the mutual ring positions (H4−C4−C4′−H4′ dihedral angles; Table 3).

In the next step, we tried to change a single piperidine ring conformation in the most stable **7a** conformer. According to our results, the system with an axial N−O bond is unstable and the same holds for its boat conformation according to the N1−C4 axis. We have found only one stable boat conformation, **7d**, according to a C2−C5 axis (Figure S15 in Supporting Information) with two significantly different A_N values, but its energy is too high, and this implies its negligible concentration in solution (Table 3).

Finally, we tried to approximate the solvent effects by dichloromethane and propane molecules located near the N−O group (models **7e−h**). As can be seen, >N−O···H−$CHCl_2$ hydrogen bonds significantly affect the N−O spin density distribution, which implies higher A_N values in comparison to the >N−O···Cl−CH_2Cl values. The difference between both DFT calculated A_N values is ca. 3 times lower in comparison to experimental data (cf. Table 2), because DFT methods underestimate weak interactions. Our results indicate a comparable abundance of the symmetric **7e0** model with two hydrogen bonds (Figure S16 in the Supporting Information) and the asymmetric **7f0** model with a single hydrogen bond in a dichloromethane solution (the energy of the **7g0** model without hydrogen bonds is too high). On the other hand, the large energy difference between analogous adducts of **2** with dichloromethane (**2b0** and **2c0** models) implies the dominant abundance of the **2b0** model with the hydrogen bond (see Table 3).

MP2 calculations on **2b0**, **2c0** and **7e0**−**7g0** model systems confirmed the above DFT results on their relative abundance in dichloromethane solutions (Table 3). On the other hand, the MP2 method produces overly high A_N values, despite the fact that their differences are very close to the experimental differences.

As expected, the DFT method used (especially without inclusion of solvent effects) produces lower A_N values in comparison to experimental data, whereas the MP2 values are overestimated. Nevertheless, our results indicate that the asymmetry in experimental EPR spectra of **7** in dichloromethane cannot be explained by the existence of its various conformers in solution but rather by the differences between >N−O···H−$CHCl_2$ and >N−O···Cl−CH_2Cl interactions.

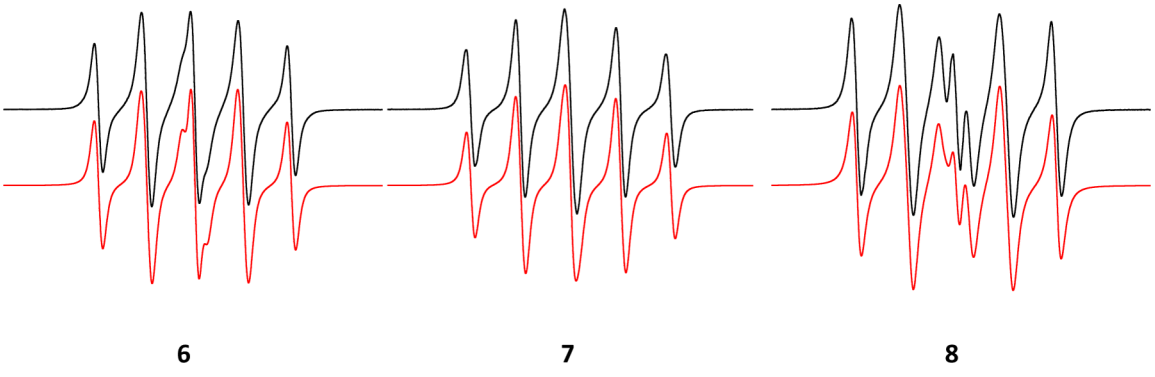

Figure 5. Experimental (black —) and simulated (red —) X-band EPR spectra of dinitroxides **6**−**8** obtained at 295 K in dichloromethane: magnetic field sweep 6 mT; dinitroxide concentration 0.1 mM. Spin Hamiltonian parameters elucidated from simulations are summarized in Table 2.

dx.doi.org/10.1021/jo400845m | J. Org. Chem. XXXX, XXX, XXX−XXX

Table 3. Model System Notations, Mutual Ring Orientations, Relative Free Energies at 298 K (ΔG_{298}), NO Spin Densities (ρ_N and ρ_O), Corresponding Hyperfine Coupling Constants (A_N), and Relative Abundances (N_{rel})

nitroxide	M_S	solvent	model	H4−C4−C4′−H4′ angle (deg)	ΔG_{298} (kJ/mol)	ρ_N	ρ_O	A_N (mT)	N_{rel}
				B3LYP Method					
2	2		**2a0**			0.432	0.524	1.521	
2	2	CH_2Cl_2	**2a1**			0.460	0.497	1.583	
2	2	n-C_7H_{16}	**2a2**			0.446	0.511	1.539	
2···H−$CHCl_2$	2		**2b0**		0.00[a]	0.465	0.485	1.585	1.000[a]
2···Cl−$CClH_2$	2		**2c0**		10.71[a]	0.441	0.509	1.539	0.013[a]
7	3		**7a0**	81.8	0.00[b]	0.431	0.524	1.523	1.000[b]
7	3		**7b0**	25.1	5.78[b]	0.430	0.524	1.526	0.098[b]
7	3		**7c0**	166.8	12.76[b]	0.430	0.524	1.526	0.006[b]
7	3		**7d0**[c]	12.5	17.56[b]	0.430, 0.450	0.521, 0.524	1.529, 1.275	0.001[b]
7	3	CH_2Cl_2	**7a1**	81.2	0.00[d]	0.460	0.497	1.578	1.000[d]
7	3	CH_2Cl_2	**7b1**	28.5	−1.58[d]	0.459	0.460	1.591	1.892[d]
7	3	CH_2Cl_2	**7c1**	167.1	9.45[d]	0.459	0.497	1.587	0.022[d]
7	3	CH_2Cl_2	**7d1**[c]	10.8	19.43[d]	0.460, 0.480	0.492, 0.497	1.589, 1.368	0.004[d]
7	3	n-C_7H_{16}	**7a2**	82.8	0.00[e]	0.445	0.511	1.550	1.000[e]
7	3	n-C_7H_{16}	**7b2**	26.2	3.81[e]	0.444	0.510	1.555	0.214[e]
7	3	n-C_7H_{16}	**7c2**	166.8	12.21[e]	0.443	0.512	1.565	0.007[e]
7	3	n-C_7H_{16}	**7d2**[c]	13.6	20.69[e]	0.444, 0.465	0.507, 0.511	1.557, 1.330	0.002[e]
Cl_2HC−H···**7**···H−$CHCl_2$	3		**7e0**	80.0	0.00[f]	0.463	0.488	1.573	1.000[f]
Cl_2HC−H···**7**···Cl−CH_2Cl	3		**7f0**	83.0	3.36[f]	0.440, 0.462	0.510, 0.491	1.538, 1.564	0.257[f]
ClH_2C−Cl···**7**···Cl−CH_2Cl	3		**7g0**	77.5	16.38[f]	0.440	0.511	1.531	0.001[f]
C_3H_8···**7**···H_8C_3	3		**7h0**	81.4		0.439	0.513	1.532	
				MP2 Method					
2···H−$CHCl_2$	2		**2b0**		0.00[a]	0.604	0.380	2.295	1.000[a]
2···Cl−$CClH_2$	2		**2c0**		12.09[a]	0.606	0.382	2.381	0.008[a]
Cl_2HC−H···**7**···H−$CHCl_2$	3		**7e0**		0.00[f]	0.602	0.382	2.286	1.000[f]
Cl_2HC−H···**7**···Cl−CH_2Cl	3		**7f0**		0.94[f]	0.605, 0.597	0.382, 0.388	2.370, 2.232	0.683[f]
ClH_2C−Cl···**7**···Cl−CH_2Cl	3		**7g0**		22.51[f]	0.597	0.393	2.342	<0.001[f]

[a]Related to the **2b0** model. [b]Related to the **7a0** model. [c]Different chair conformations of both rings. [d]Related to the **7a1** model. [e]Related to the **7a2** model. [f]Related to the **7e0** model.

X-ray Diffraction Studies. To get a detailed insight into the molecular and bulk structures of the studied nitroxides in the solid phase, the X-ray analyses of single crystals of **4**−**8** were performed (Table 4 and the Supporting Information).

The crystal structures of nitroxides **4**−**8** are depicted in Figures 6−10 (for their ORTEP drawings and/or packing diagrams see Figures S17−S21 in the Supporting Information). As expected, the piperidine rings in all of these compounds exhibit a chair conformation, while the pyrrolidine ring in **6** has an envelope conformation. Due to the presence of a methanesulfonyl group, molecules of nitroxide **4** (Figure 6) in the packing are linked in chains through weak interactions between O4 and H10A with an interatomic distance of 2.326 Å. Similarly, and due to the presence of a sulfonamide group in the nitroxide **5**, there are two intermolecular hydrogen bonds (Figure 7) formed by sulfonyl O3 and amino H2A from one molecule and the same pair of the atoms from the second molecule at a distance of 2.43 Å (symmetry code $-x + 2, -y, -z + 1$). On the other hand, nitroxide **6** features an intermolecular hydrogen bond (Figure 8) between the PROXYL nitroxyl O2 and amino H1A at a distance of 2.26 Å (symmetry code $-x + 1, y + {}^1/_2, -z$). Due to the poor crystallinity of nitroxide **7**, the molecular structure was determined by a single-crystal X-ray analysis of its ammonium salt **7′** in the form of acetate (Figure 9), prepared by slow evaporation of a DCM/AcOEt solution of **7** at room temperature. There is a hydrogen bond formed by the amino H1 and acetyl O2 at a distance of 1.789 Å. Finally, molecules of nitroxide **8** in the packing are linked in a chain (Figure 10) through a weak stabilization interaction between nitroxyl O1 and methanesulfonyl H19A (interatomic distance of 2.573 Å with symmetry codes $x, y, 1 + z$ and $x, y, -1 + z$). Moreover, the crystal structures of all studied nitroxides **4**−**8** possess two common characteristic features: (a) oxygen atoms of N−O radical sites are located close to methyl and/or methylene H atoms at β positions of adjacent molecules with intermolecular O···H distances close to the sum of van der Waals radii (2.6 Å)[30] (Table S2 in the Supporting Information); (b) N1−O1 distances of the nitroxyl moieties are shortened in comparison to those in TEMPO[31] (Table 5).

Magnetic Measurements. The solid state of nitroxide **4** consists of monoradical species. The effective magnetic moment refers to a Curie paramagnet: $\mu_{eff} < 2\ \mu_B$ (Figure 11). Low-temperature susceptibility and its inverse indicate a presence of a maximum (minimum) that is a fingerprint of the chainlike behavior. The fitting procedure to the model of a regular $S = {}^1/_2$ Heisenberg chain gave $g = 2.001$, isotropic exchange coupling constant $J/hc = -2.15\ cm^{-1}$, temperature-independent magnetism $\chi_{TIM} = -2.73 \times 10^{-9}\ m^3\ mol^{-1}$, molecular-field correction $(zj)/hc = -1.24\ cm^{-1}$, and discrepancy factor for the susceptibility $R(\chi) = 0.0091$. It can be seen that the fit is almost perfect for the magnetic susceptibility and/or its inverse. However, the magnetization stays unfitted, since there are neither closed formulas nor a

dx.doi.org/10.1021/jo400845m | J. Org. Chem. XXXX, XXX, XXX−XXX

Table 4. Crystallographic Data from Single-Crystal X-ray Analyses of Nitroxides 4−8

	4	5	6	7′	8
empirical formula	$C_{10}H_{20}NO_4S$	$C_{10}H_{21}N_2O_3S$	$C_{17}H_{33}N_3O_2$	$C_{20}H_{39}N_3O_4$	$C_{19}H_{37}N_3O_4S$
formula wt	250.33	249.35	311.46	385.29	403.58
temp, K	293(2)	293(2)	293(2)	293(2)	100(2)
wavelength, Å	0.71073	0.71073	0.71073	1.54184	0.71073
cryst syst; space group	monoclinic; $P2_1/c$	monoclinic; $P2_1/c$	monoclinic; $P2_1$	tetragonal; $P\bar{4}n2$	orthorhombic; $Fdd2$
a, Å	12.9484(6)	6.3108(3)	7.8821(8)	11.8431(1)	41.422(1)
b, Å	9.9797(3)	21.6752(8)	11.6183(7)	11.8431(1)	21.0998(6)
c, Å	11.1310(4)	11.2066(5)	10.8273(8)	19.1284(4)	10.1443(3)
β, deg	113.437(5)	119.167(3)	111.061(1)		
V, Å^{-3}	1319.69(9)	1338.6(1)	925.3(1)	2682.93(6)	8866.1(4)
Z; calcd density, Mg m^{-3}	4; 1.260	4; 1.237	2; 1.118	8; 0.954	16; 1.209
abs coeff, mm^{-1}	0.245	0.238	0.073	0.531	0.174
F(000)	540	540	344	848	3520
cryst size, mm^{-3}	0.420 × 0.477 × 0.853	0.686 × 0.903 × 1.104	0.257 × 0.303 × 0.481	0.663 × 0.127 × 0.115	0.95 × 0.70 × 0.46
θ range for data collection, deg	3.66−29.56	4.11−26.37	4.34−26.37	4.39−76.03	2.67−28.18
no. of collected/unique rflns	21523/3391 (R(int) = 0.0193)	19947/2716 (R(int) = 0.0171)	14911/3774 (R(int) = 0.0207)	58185/2804 (R(int) = 0.0438)	44036/5160 [(R(int) = 0.0399)
completeness to 2θ = 25.00, %	99.8	99.6	99.4	100	99.9
abs cor	analytical				
refinement method	full-matrix least squares on F^2				
no. of data/restraints/params	3391/0/146	2716/0/145	3774/1/202	2804/1/129	5160/1/244
GOF on F^2	1.030	1.185	1.046	1.095	1.043
final R indices ($I > 2\sigma(I)$)	R1 = 0.0405, wR2 = 0.1059	R1 = 0.0383, wR2 = 0.1241	R1 = 0.0386, wR2 = 0.1015	R1 = 0.0370, wR2 = 0.1086	R1 = 0.0351, wR2 = 0.0961
R indices (all data)	R1 = 0.0508, wR2 = 0.1126	R1 = 0.0412, wR2 = 0.1269	R1 = 0.0427, wR2 = 0.1046	R1 = 0.0397, wR2 = 0.1114	R1 = 0.0357, wR2 = 0.0967
$\Delta\rho_{max}$ and $\Delta\rho_{min}$, e, Å^{-3}	0.254 and −0.415	0.407 and −0.359	0.152 and −0.134	0.085 and −0.083	0.227 and −0.208

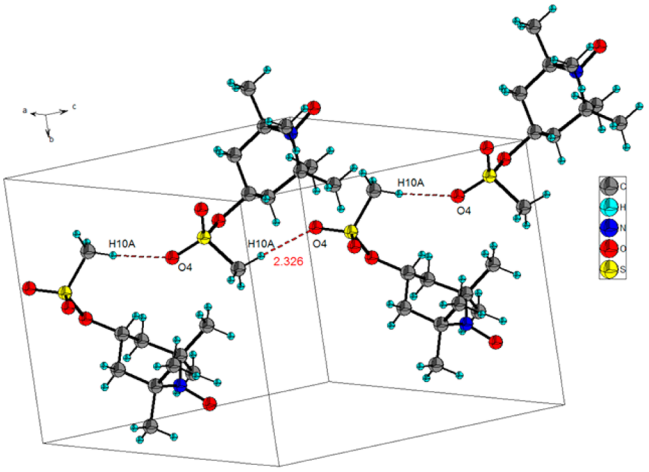

Figure 6. Weak intermolecular interactions between molecules of nitroxide **4**.

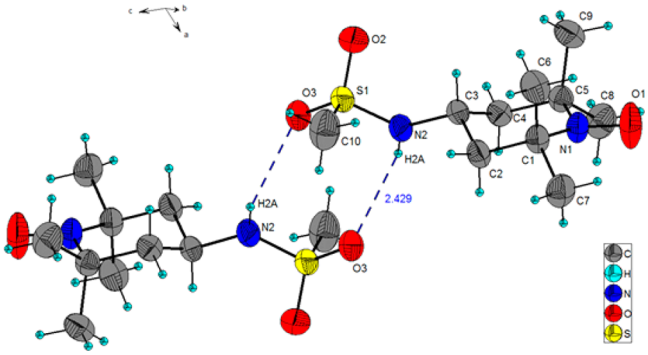

Figure 7. ORTEP drawing of nitroxide **5** and its intermolecular hydrogen bonds.

rigorous approach for an infinite system at our disposal. The only way is to mimic the chainlike properties by a finite ring approximation with even and odd members at finite temperature.[29] The solid state of nitroxide **5** consists of monoradical species as well. The effective magnetic moment refers to a Curie paramagnet: $\mu_{eff} < 2\ \mu_B$ (Figure 11). Low-temperature susceptibility and its inverse indicate the presence of a maximum (minimum) that is a fingerprint of the antiferromagnetic chain. The magnetization per formula unit does not saturate at $B = 7$ T and $T = 2.0$ K; this again indicates a chainlike behavior. The fitting procedure to the model of a regular $S = {}^1/_2$ Heisenberg chain gave $g = 2.041$, $J/hc = -3.05$ cm^{-1}, $\chi_{TIM} = -1.86 \times 10^{-9}$ m^3 mol^{-1}, $(zj)/hc = -0.141$ cm^{-1}, and $R(\chi) = 0.0036$.

The solid state of nitroxide **6** exhibits features of a biradical (Figure 12) constituted of $[S_1, S_2] = [{}^1/_2, {}^1/_2]$ spins: the room-temperature effective magnetic moment is $\mu_{eff} = 2.32\ \mu_B$, which matches the value for two uncoupled spins (2.45 for $g = 2$). When the temperature is lowered, the susceptibility passes through a maximum and then decreases. However, at very low temperature a contamination with uncoupled magnetic centers is visible. The magnetization data reflect a presence of that paramagnetic impurity. The fitting procedure for a model of exchange interaction between two spins with $\hat{H}^{ex} = -J(\vec{S}_1 \cdot \vec{S}_2)$ gave the following: exchange coupling constant $J/hc = -8.68$ cm^{-1}, $g = 1.93$, mole fraction of the paramagnetic impurity x_{PI} =

dx.doi.org/10.1021/jo400845m | J. Org. Chem. XXXX, XXX, XXX−XXX

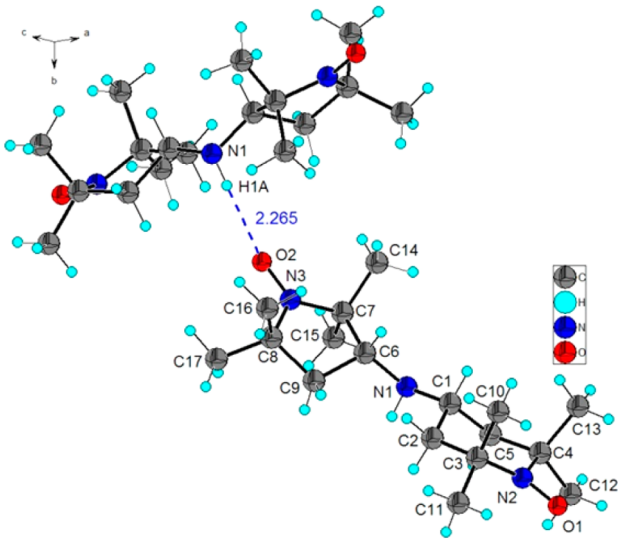

Figure 8. ORTEP drawing of nitroxide **6** and its weak bimolecular interaction.

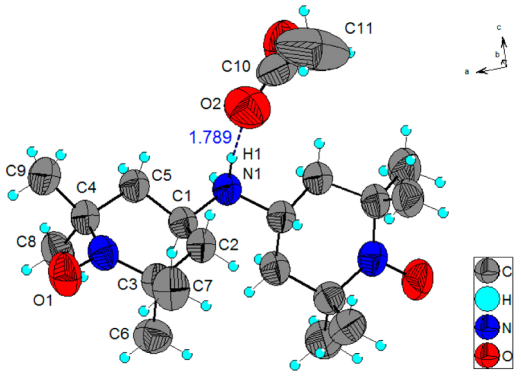

Figure 9. ORTEP drawing of nitroxide 7′. Labels are given for independent atoms only. Acetate anion and voids (for water molecule) are omitted for clarity.

0.127, $\chi_{TIM} = -0.93 \times 10^{-9}$ m^3 mol^{-1}, $(zj)/hc = -0.879$ cm^{-1}, $R(\chi) = 0.011$, $R(M) = 0.090$. Only a weak intermolecular interaction of an antiferromagnetic nature is detected.

The solid state of nitroxide **7** represents a biradical system as well (Figure 12). The final set of magnetic parameters is as follows: $J/hc = -2.23$ cm^{-1}, $g = 2.00$, $\chi_{TIM} = -2.91 \times 10^{-9}$ m^3 mol^{-1}, $(zj)/hc = -0.164$ cm^{-1}, $R(\chi) = 0.046$, $R(M) = 0.097$.

Table 5. Comparison of N−O Bond Lengths Obtained from X-ray Analyses

nitroxide	N−O bond length (Å)
TEMPO	1.294(4)
4	1.280(2)
5	1.277(2)
6	1.277(2)
7′	1.285(2)
8	1.285(2)

Owing to the small value of the exchange coupling constant, a maximum at the susceptibility curve is not seen until the lowest temperature reached during the data acquisition.

Finally, the solid state of nitroxide **8** refers to the biradical $[S_1, S_2] = [^1/_2, ^1/_2]$ (Figure 12). The effective magnetic moment on cooling behaves like a Curie paramagnet with some temperature-independent magnetism χ_{TIM} (negative, owing to uncompensated diamagnetism of the specimen). Since no maximum at the susceptibility curve is visible down to $T = 2.0$ K, the exchange coupling constant should be small and negative. The magnetization per formula unit nearly saturates at $B = 7$ T and $T = 2.0$ K to the value of $M_1 = 2\ \mu_B$; this supports the model of a isolated biradical. The fitting procedure gave the following: $J/hc = -1.50$ cm^{-1}, $g = 2.00$, $\chi_{TIM} = -5.81 \times 10^{-9}$ m^3 mol^{-1}, $(zj)/hc = -0.069$ cm^{-1}, $R(\chi) = 0.029$, $R(M) = 0.030$. Only a weak intermolecular interaction of an antiferromagnetic nature is detected.

CONCLUSIONS

In conclusion, a comparison set of five mono-/biradical TEMPO derivatives **4**−**8** was prepared. All compounds were fully characterized and their structures determined by single-crystal X-ray analyses. The spin, magnetic, and redox properties of novel compounds were studied by means of EPR spectroscopy, SQUID magnetometry, and cyclic voltammetry. Regarding CV, all studied nitroxides undergo a reversible one-electron-transfer process with half-wave potentials in the range of 401−616 mV. The results indicate an emerging trend that the electron-withdrawing substituents tend to increase the oxidation potential of a nitroxide in comparison to electron-donating groups. While EPR spectra of monoradicals **1**, **2**, **4**, and **5** in DCM revealed the expected three-line signal, spectra of biradicals **6**−**8** showed more complex features. Interestingly, symmetric biradicals **7** and **8** exhibit five-line spectra analogous to the that of the nonsymmetric **6**. Results of DFT and MP2

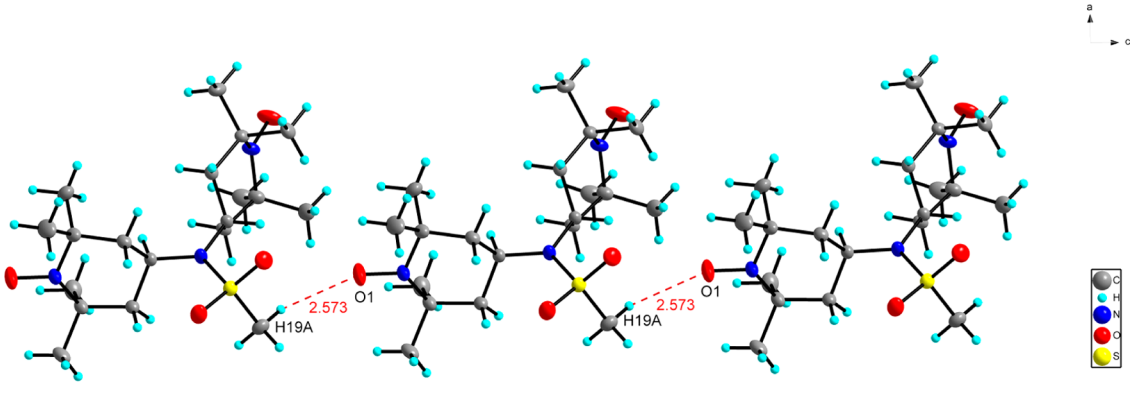

Figure 10. Packing diagram of nitroxide **8** and its weak bimolecular interactions.

dx.doi.org/10.1021/jo400845m | J. Org. Chem. XXXX, XXX, XXX−XXX

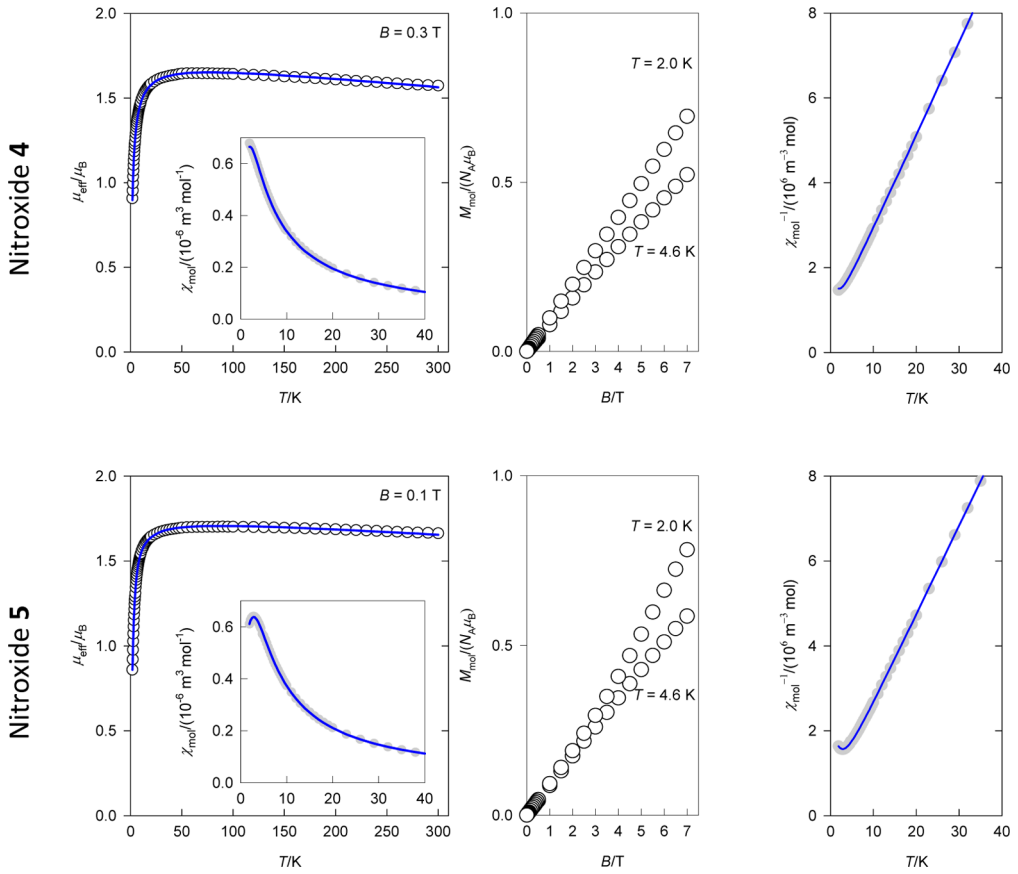

Figure 11. Magnetic data for nitroxides **4** and **5**: (left) temperature dependence of the effective magnetic moment; (center) field dependence of the magnetization; (right) inverse susceptibility. Circles denote experimental data, and solid lines are fitted with a model of an $S = {}^1/_2$ regular Heisenberg chain.[32,33]

calculations indicate that the EPR splitting patterns of **7** in DCM could be explained by differences between the >N−O···H−$CHCl_2$ and >N−O···Cl−CH_2Cl interactions with solvent molecules. In the solid state, mononitroxides **4** and **5** behave as a Heisenberg antiferromagnetic chain, whereas dinitroxides **6**−**8** are almost isolated paramagnetic diradicals coupled in an antiferromagnetic manner. Moreover, the crystal structures of all studied nitroxides **4**−**8** possess two common characteristic features: (a) oxygen atoms of N−O radical sites are located close to methyl and/or methylene H atoms at β positions of adjacent molecules with intermolecular O···H distances close to the sum of van der Waals radii (2.6 Å); (b) N1−O1 distances of the nitroxyl moieties are shortened in comparison to those in TEMPO.

EXPERIMENTAL SECTION

General Considerations. Commercially available TEMPO and nitroxides **1**−**3** were purchased. All solvents of p.a. purity were dried over 4 Å molecular sieves. All reagents were purchased and used as received without further purification. Thin-layer chromatography (TLC) was performed on aluminum plates precoated with 0.2 mm silica gel 60 F254. Flash column liquid chromatography (FLC) was performed on Kieselgel 60 (40−63 μm). Infrared (IR) spectra were recorded on a FTIR spectrometer as films on a diamond sampler (ATR). Melting points were determined on a capillary apparatus and are uncorrected. Liquid chromatography−mass spectrometry (LC-MS) analyses were performed on an instrument equipped with a multimode MS detector using the MM ESI/APCI ionization method (column Zorbax SB C-8 12.5 2.1 mm, particle size 5 μm, eluent water/MeOH with 0.1% HCO_2H, gradient 0−100% of MeOH for 2.5 min, flow 1.5 mL/min). HRMS spectra were recorded on a TOF-Q instrument and evaluated using Compass DataAnalysis 4.0 software. Elemental analysis was carried out at the Department of Inorganic Chemistry, Slovak University of Technology.

2,2,6,6-Tetramethyl-4-(methylsulfonyloxy)piperidine *N*-Oxide (4). Triethylamine (6.663 g, 4.50 mL, 58.17 mmol) was added to a cooled (ice bath) solution of 4-hydroxy-TEMPO **2** (5.000 g, 29.08 mmol) in DCM (80 mL) under Ar. After 5 min, methanesulfonyl chloride (5.885 g, 8.06 mL, 58.17 mmol) was added dropwise with stirring and the reaction temperature continuously rised to 20 °C. After 2 h of stirring at room temperature, the DCM solution was washed with water (2 × 80 mL) and a saturated aqueous $NaHCO_3$ solution (35 mL), and the separated organic layer was dried over anhydrous $MgSO_4$. The filtration of solids, evaporation of volatiles in vacuo, addition of ethyl acetate (5 mL), and final filtration of the solution through a short pad of silica gel (0.5 × 2 cm, eluting with EtOAc) afforded mesylate **4** (5.857 g, 80%) as a deep red crystalline solid. Slow evaporation from its DCM or EtOAc solution afforded deep red crystals of **4** suitable for X-ray analysis (Figure S17, Supporting Information).

Data for **4**: R_f = 0.32 (EtOAc/toluene 1/3); mp 94−95 °C (lit.[34] mp 94 °C); IR (ATR): ν_{max} 3033, 2981, 2941, 1468, 1346, 1339, 1169, 933, 870, 828, 525, 501 cm^{-1}; MS (*m*/*z*) 251.3 $[M + 1]^+$. Anal. Calcd for $C_{10}H_{20}NO_4S^{\bullet}$ (250.34): C, 47.98; H, 8.05; N, 5.60; S, 12.81. Found: C, 47.71; H, 7.93; N, 5.52; S, 12.79.

2,2,6,6-Tetramethyl-4-(methylsulfonylamino)piperidine *N*-Oxide (5). In a modification of the previously described procedure,[15] compound **5** was prepared via the following two-step protocol. Thus, 4-amino-2,2,6,6-tetramethylpiperidine (500 mg, 556 μL, 3.20 mmol) was dissolved in DCM (30 mL) and methanesulfonyl chloride (367 mg, 248 μL, 3.20 mmol) was added dropwise with stirring at room temperature. After 1 h, the precipitated solids were filtered off, washed

dx.doi.org/10.1021/jo400845m | J. Org. Chem. XXXX, XXX, XXX−XXX

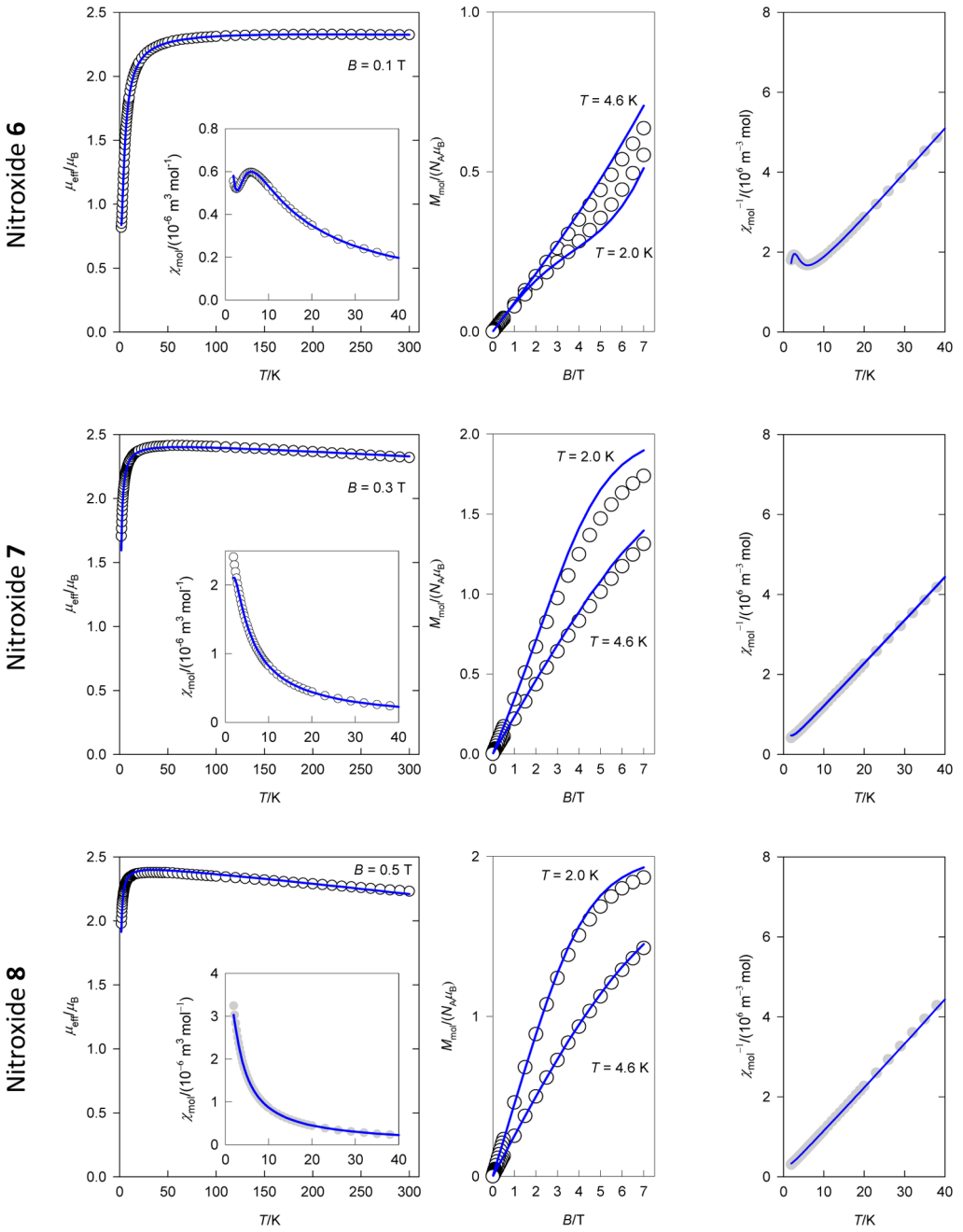

Figure 12. Magnetic data for nitroxides **6**–**8**: (left) temperature dependence of the effective magnetic moment; (center) field dependence of the magnetization; (right) inverse susceptibility. Circles denote experimental data, and solid lines are fitted with a model of isolated biradicals [S_1, S_2] = [$^1/_2$, $^1/_2$].

with DCM (10 mL), and dried in vacuo to give the mesylated product as the hydrochloride **9** (859 mg). This salt was dissolved in MeOH/H_2O (10 + 5 mL), and a saturated aqueous $NaHCO_3$ solution (4 mL) was added. Next, $Na_2WO_4{\cdot}2H_2O$ (211 mg, 0.64 mmol) and 30% aqueous H_2O_2 solution (983 μL, 32 mmol, 10 equiv) were added sequentially to the resulting solution. The reaction mixture was stirred at room temperature for 4 h. Then, water (30 mL) and DCM (30 mL) were added, the mixture was stirred for 5 min, and the separated water layer was re-extracted with DCM (20 mL). The combined organic extracts were dried over anhydrous $MgSO_4$, filtered, and evaporated in vacuo. The obtained crude product was purified by FLC (SiO_2, gradient elution with hexanes/AcOEt from 1/0 to 1/1) to afford the light orange solid product **5** (676 mg, 85%). Slow crystallization from its EtOAc/hexanes solution (1/1) afforded red crystals of **5** suitable for X-ray analysis (Figure 7).

Data for **5**: R_f = 0.21 (EtOAc/hexanes 1/1); mp 141–143 °C (lit.[15] mp 141–143 °C); IR (ATR) ν_{max} 3275, 2979, 2941, 1436, 1361, 1330, 1318, 1299, 1153, 1067, 985, 767, 523, 485 cm^{-1}; MS (*m*/*z*) 250.2 [M + 1]$^+$. Anal. Calcd for $C_{10}H_{21}N_2O_3S^{\bullet}$ (249.35): C, 48.17; H, 8.49; N, 11.23; S, 12.86. Found: C, 48.31; H, 8.47; N, 11.23; S, 12.68.

***N*-(1-Oxido-2,2,6,6-tetramethylpiperidin-4-yl)-*N*-(1-oxido-2,2,5,5-tetramethylpyrolidin-3-yl)amine (6).** A solution of 3-amino-PROXYL (100 mg, 0.64 mmol) and 4-oxo-TEMPO (108 mg, 0.64 mmol) in MeOH (2 mL) was acidified with 3 drops of glacial AcOH in a pressure tube under Ar. After the mixture was stirred for 20 min, $NaBH_3CN$ (80 mg, 1.27 mmol) was added and the reaction vessel was heated in an oil bath at 80 °C for 24 h. The solution was cooled to room temperature, and water (2 mL) and DCM (2 mL) were added. The organic layer was separated, and the water phase was extracted with DCM (2 × 2 mL). The combined organic layers were

dx.doi.org/10.1021/jo400845m | J. Org. Chem. XXXX, XXX, XXX–XXX

dried over anhydrous $MgSO_4$ and filtered, and the solvent was evaporated in vacuo. The crude product was purified by FLC (SiO_2, gradient elution with DCM/MeOH from 1/0 to 9/1) to give biradical **6** (91 mg, 46%) as a yellow-orange crystalline solid. Slow crystallization from an EtOAc/hexanes mixture via the diffusion method afforded deep orange crystals of **6** suitable for X-ray analysis (Figure 8).

Data for **6**: R_f = 0.59 (EtOAc); mp 161−163 °C; IR (ATR) ν_{max} 3294, 2974, 2938, 2868, 1462, 1359, 1174, 1129, 801, 769, 530 cm^{-1}; MS (*m/z*) 312.3 $[M+1]^+$. Anal. Calcd for $C_{17}H_{33}N_3O_2^{\bullet\bullet}$ (311.46): C, 65.56; H, 10.68; N, 13.49. Found: C, 65.73; H, 10.55; N, 13.47.

***N,N*-Bis(1-oxido-2,2,6,6-tetramethylpiperidin-4-yl)amine (7).** 4-Oxo-TEMPO **1** (496 mg, 2.92 mmol) was added to a solution of 4-amino-TEMPO (500 mg, 2.92 mmol) in anhydrous MeOH (12 mL) under Ar. After the mixture was stirred for 5 min, acetic acid (5 drops) was added and the resulting solution was stirred for 20 min. Next, sodium borohydride (366 mg, 5.84 mmol) was added at once and the mixture was refluxed for 50 h. The reaction mixture was then diluted with DCM (20 mL), and saturated aqueous $NaHCO_3$ solution (10 mL) with water (10 mL) was added. The separated water layer was extracted with DCM (20 mL). The combined organic phases were dried over anhydrous $MgSO_4$, the solids were filtered off, the volatiles were evaporated in vacuo, and the residue was purified by FLC (SiO_2, gradient elution with hexanes/EtOAc from 4/1 to 1/0) to furnish **7** (608 mg, 64%) as a red-orange solid. Slow evaporation from a DCM/EtOAc solution (1/2) afforded bright red crystals of the ammonium salt **7′** suitable for X-ray analysis (Figure 9).

Data for **7**: R_f = 0.58 ($CHCl_3$/EtOAc/MeOH 7/3/1); mp 154−156 °C (lit.[17] mp 156−158 °C); IR (ATR) ν_{max} 3435, 3298, 2972, 2932, 2866, 1666, 1457, 1375, 1358, 1242, 1180, 1116, 700, 567, 558, 497 cm^{-1}; MS (*m/z*) 326.3 $[M + 1]^+$; HRMS mass calcd for $C_{18}H_{35}N_3O_2^{\bullet\bullet}$ $[M + H]^+$ 326.2808, found 326.2565, $[M + Na]^+$ calcd 348.2627, found 348.2621. Anal. Calcd for $C_{18}H_{35}N_3O_2^{\bullet\bullet}$ (325.49): C, 66.42; H, 10.84; N, 12.91. Found: C, 66.74; H, 10.71; N, 12.87.

Methanesulfonyl-*N,N*-bis(1-oxido-2,2,6,6-tetramethylpiperidin-4-yl)amide (8). Diisopropylethylamine (401 mg, 541 mL, 3.07 mmol) was added to a solution of **7** (100 mg, 0.31 mmol) in anhydrous DCM (4 mL) at 0 °C (ice bath) under Ar in a sealable tube. After the mixture was stirred for 5 min, methanesulfonic acid anhydride (268 mg, 1.54 mmol) was added portionwise at 0 °C over a period of 5 min and the reaction temperature continuously rose to 20 °C for 2 h. After the solution was stirred for an additional 16 h at 60 °C, the reaction was stopped by addition of water (2 mL). DCM (10 mL) was added, and the organic layer was washed with water (2 × 10 mL) and saturated aqueous $NaHCO_3$ solution (5 mL) and dried over anhydrous $MgSO_4$. The solids were filtered off, the volatiles were evaporated in vacuo, and the residue was purified by FLC (SiO_2, gradient elution with hexanes/EtOAc from 10/1 to 1/1) to furnish mesylate **8** (44 mg, 35%) as an orange solid. Slow crystallization from a hexanes/EtOAc mixture via the diffusion method afforded red crystals of **8** suitable for X-ray analysis (Figure S21, Supporting Information).

Data for **8**: R_f = 0.64 (EtOAc/Hex 1/1); mp 192−195 °C; IR (ATR) ν_{max} 2978, 2937, 1734, 1471, 1322, 1199, 1152, 1019, 955, 802, 743, 517 cm^{-1}; MS (*m/z*) 404.3 $[M + 1]^+$; HRMS mass calcd for $C_{19}H_{37}N_3O_4S^{\bullet\bullet}$ $[M + Na]^+$ 426.2397, found 426.2693, $[2M + Na]^+$ calcd 829.4998, found 829.4446. Anal. Calcd for $C_{19}H_{37}N_3O_4S^{\bullet\bullet}$ (403.58): C, 56.54; H, 9.24; N, 10.41; S, 7.95. Found: C, 56.63; H, 9.14; N, 10.38; S, 7.82.

Cyclic Voltammetry. *Chemicals.* Stock solutions of compounds **1**−**8** ($c = 1 \times 10^{-3}$ mol L^{-1}) in H_2O/MeOH (9/1 v/v) were used for the preparation of working solutions (1×10^{-4} mol L^{-1}) for electrochemical measurements by dilution with aqueous phosphate buffer (PBS) at pH 7 as supporting electrolyte. The latter was prepared from a mixture of monosodium phosphate (NaH_2PO_4) and disodium phosphate (Na_2HPO_4) according to the literature.[35] All chemicals (analytical-reagent grade) were used without further purification. The aqueous solutions were made with double-distilled deionized water with resistivity above 18 MΩ cm.

Electrochemical Measurements. The cyclic voltammetry (CV) measurements were performed using a PGSTAT-302N potentiostat/galvanostat equipped with a USB electrochemical interface connected to a three-electrode single-compartment glass cell and personal computer for data storage and processing. NOVA 1.8 software was employed for elaboration and evaluation of all CV voltammograms. The glass electrochemical cell consisted of Ag/AgCl (3 mol L^{-1} KCl) and Pt wire as reference and counter electrodes, respectively. A paraffin-impregnated graphite electrode (PIGE) with a diameter of 5 mm was used as the working electrode. The PIGE was polished with aluminum oxide (grain size 0.3 μm) and rinsed with deionized water to obtain a fresh electrode surface before each experiment. The pH value of PBS was monitored with a pH meter with a combined glass electrode, which was regularly calibrated with standard buffer solutions. All of the half-wave potentials ($E_{1/2}$) are given against Ag/AgCl (3 mol L^{-1} KCl) at an ambient temperature of 25 ± 1 °C. A 20 mL portion of the supporting electrolyte containing an appropriate amount of the studied compound was added to the glass electrochemical cell. Before each measurement, ultrapure N_2 (O_2 <2 ppm) was used to degas the solutions (10 min) and to provide an inert atmosphere inside the electrochemical cell. CV voltammograms were recorded in a potential range from −1.5 to +1 V and from 0 to +1 V, respectively. The optimized instrumental CV parameters were as follows: scan rate of 100 mV s^{-1}, step potential of 5 mV, and interval time of 0.05 s. At the beginning, the current response for a blank (PBS at pH 7 without any compound) was measured to check the electrochemical background of the system. CV voltammograms of each studied species were carried out 5-fold (n = 5), and the average scan was considered for the evaluation of $E_{1/2}$ and construction of the CV figures.

Electron Paramagnetic Resonance. The stock solutions of all nitroxides were prepared in dichloromethane (maximum 0.004% H_2O). EPR spectra were measured with freshly diluted solutions ($c \approx$ 0.1 mM) carefully saturated with Ar and immediately transferred to a small quartz flat cell optimized for the TE_{102} cavity. The X-band spectra were recorded using an EPR spectrometer at a temperature of 295 K. The experimental g values were determined using a built-in magnetometer. Typical EPR spectrometer settings were as follows: microwave frequency 9.428 GHz; microwave power 10.53 mW; center field 335.8 mT; sweep width 6−10 mT; gain 5×10^3; modulation amplitude 0.02 mT; scan 82 s; time constant 10.24 ms; number of scans 5. The experimental EPR spectra were analyzed and simulated using the WinEPR and SimFonia, Winsim2002 software.[36] The simulated spectra of dinitroxides were calculated with the EasySpin software package[25] using the fitting function *pepper* suitable for the exchange coupling constant calculations in systems with $S > {}^1/_2$. The spin Hamiltonian parameters were optimized by nonlinear least-squares methods to obtain the best agreement between experimental and calculated spectra.

Quantum-Chemical Calculations. The geometries of the neutral systems under study were optimized without any symmetry restrictions at the DFT level of theory (B3LYP hybrid functional)[37] and some of them also at the MP2[38] (with all electrons included in a correlation calculation) level of theory using standard cc-pVDZ basis sets[39] from the GAUSSIAN03 library.[40] The stability of the obtained structures has been tested by vibrational analysis (no imaginary vibrations). The solvent effects of dichloromethane and *n*-heptane were estimated by single solvent molecules in the vicinity of $NO^{\bullet}$ groups (using propane molecules instead of the *n*-heptane) and alternatively by using the polarizable conductor calculation model (CPCM).[41] The values of isotropic hyperfine coupling constants were evaluated in terms of Fermi contact interactions.[42,43] Their values for the systems containing two unpaired electrons have been doubled.[44] All calculations have been performed using the GAUSSIAN03 program package.[40] Relative abundances of individual model systems were evaluated using Boltzmann distributions and their free energy data at room temperature.

X-ray Analyses. X-ray diffraction data were collected on a diffractometer equipped with a ruby CCD detector and Mo Kα and Cu Kα sealed-tube sources at room temperature. Data reduction was

dx.doi.org/10.1021/jo400845m | J. Org. Chem. XXXX, XXX, XXX−XXX

performed with CrysAlis RED (version 1.171.36.20) software.[45] Crystal structures were solved and refined with SHELXS97.[46] The DIAMOND program was used for the molecular graphics.[47]

Magnetic Measurements. The experimental data were taken with a SQUID magnetometer using the RSO mode of detection with ca. 20 mg of the sample encapsulated in a gelatin sample holder. The magnetic susceptibility taken at $B = 0.5$ T has been corrected for the underlying diamagnetism and converted to the effective magnetic moment. The magnetization has been measured at two temperatures: $T = 2.0$ and $T = 4.6$ K.

■ ASSOCIATED CONTENT

Supporting Information

Figures, tables, and CIF files giving HRMS spectra of dinitroxides **7** and **8**, CV spectra of all studied nitroxides, EPR spectra of mononitroxides **1**, **2**, **4**, and **5**, and ORTEP drawings and/or packing diagrams of nitroxides **4**−**8** and their selected crystallographic data. This material is available free of charge via the Internet at http://pubs.acs.org.

■ AUTHOR INFORMATION

Corresponding Author

*E-mail for P.S.: peter.szolcsanyi@stuba.sk.

Notes

The authors declare no competing financial interest.

■ ACKNOWLEDGMENTS

This work was supported by the Science and Technology Assistance Agency under Contract Nos. APVV-0202-10, APVV-0014-11, and APVV-0797-11 and by the Scientific Grant Agency of the Slovak Republic VEGA (Project Nos. 1/0679/11, 1/0289/12, 1/0327/12, and 1/0051/13). We thank the HPC center at the Slovak University of Technology in Bratislava, which is a part of the Slovak Infrastructure of High Performance Computing (SIVVP Project No. 26230120002, funded by the European Region Development Funds), for computing facilities.

■ DEDICATION

Dedicated to the memory of Peter Tisovský.

■ REFERENCES

(1) Hicks, R. G.; Ed.; *Stable Radicals. Fundamentals and Applied Aspects of Odd-Electron Compounds*; Wiley: New York, 2010.
(2) (a) Oyaizu, K.; Nishide, H. *Adv. Mater.* **2009**, *21*, 2339. (b) Janoschka, T.; Hager, M. D.; Schubert, U. S. *Adv. Mater.* **2012**, *24*, 6397.
(3) Zhelev, Z.; Bakalova, R.; Aoki, I.; Matsumoto, K.; Gadjeva, V.; Anzai, K.; Kanno, I. *Chem. Commun.* **2009**, 53.
(4) Ysacco, C.; Rizzato, E.; Virolleaud, M.-A.; Karoui, H.; Rockenbauer, A.; Le Moigne, F.; Siri, D.; Ouari, O.; Griffin, R. G.; Tordo, P. *Phys. Chem. Chem. Phys.* **2010**, *12*, 5841.
(5) Dane, E. L.; Corzilius, B.; Rizzato, E.; Stocker, P.; Maly, T.; Smith, A. A.; Griffin, R. G.; Ouari, O.; Tordo, P.; Swager, T. M. *J. Org. Chem.* **2012**, *77*, 1789.
(6) Wilcox, C. S. *Pharmacol. Ther.* **2010**, *126*, 119.
(7) Wu, Y.; Hirai, Y.; Tsunobuchi, Y.; Tokoro, H.; Eimura, H.; Yoshio, M.; Ohkoshi, S.; Kato, T. *Chem. Sci.* **2012**, *3*, 3007.
(8) Cotrim, A. P.; Hyodo, F.; Matsumoto, K.; Sowers, A. L.; Cook, J. A.; Baum, B. J.; Krishna, M. C.; Mitchell, J. B. *Clin. Cancer. Res.* **2007**, *13*, 4928.
(9) Lebelev, O. L.; Kazarnovskii, S. N. *Zhur. Obshch. Khim.* **1960**, *30*, 1631.
(10) Montanari, F.; Quici, S.; Henry-Riyad, H.; Tidwell, T. T. 2,2,6,6-Tetramethylpiperidin-1-oxyl. In *Encyclopedia of Reagents for Organic Synthesis*; Wiley: New York, 2005.
(11) Han, Ch. H.; Drache, M.; Baethge, H.; Schmidt-Naake, G. *Macromol. Chem. Phys.* **1999**, *200*, 1779.
(12) Wilcox, C. S.; Pearlman, A. *Pharmacol. Rev.* **2008**, *60*, 418.
(13) Ji, J.; Kline, A. E.; Amoscato, A.; Samhan-Arias, A. K.; Sparvero, L. J.; Tyurin, V. A.; Tyurina, Y. Y.; Fink, B.; Manole, M. D.; Puccio, A. M.; Okonkwo, D. O.; Cheng, J. P.; Alexander, H.; Clark, R. S. B.; Kochanek, P. M.; Wipf, P.; Kagan, V. E.; Bayır, H. *Nat. Neurosci.* **2012**, *15*, 1407.
(14) Merbouh, N.; Bobbitt, J. M.; Brückner, Ch. *Org. Prep. Proced. Int.* **2004**, *36*, 1.
(15) Krishna, M. C.; DeGraff, W.; Hankovszky, O. H.; Sár, C. P.; Kálai, T.; Jekő, J.; Russo, A.; Mitchell, J. B.; Hideg, K. *J. Med. Chem.* **1998**, *41*, 3477.
(16) Rauckman, E. J.; Rosen, G. M.; Hord, W. W. *Org. Prep. Proced. Int.* **1977**, *9*, 53.
(17) Rosen, G. M.; Schneider, E.; Shortkroff, S.; Tsai, P.; Winalski, C. S. *J. Chem. Soc., Perkin Trans. 1* **2002**, 2663.
(18) Blinco, J. P.; Hodgson, J. L.; Morrow, B. J.; Walker, J. R.; Will, G. D.; Coote, M. L.; Bottle, S. E. *J. Org. Chem.* **2008**, *73*, 6763.
(19) Yamasaki, T.; Mito, F.; Ito, Y.; Pandian, S.; Kinoshita, Y.; Nakano, K.; Murugesan, R.; Sakai, K.; Utsumi, H.; Yamada, K. *J. Org. Chem.* **2011**, *76*, 435.
(20) Baur, E. J.; Wang, S.; Brandt, M. C. *Anal. Chem.* **1996**, *68*, 3815.
(21) Israeli, A.; Patt, M.; Oron, M.; Samuni, A.; Kohen, R.; Goldstein, S. *Free Radical Biol. Med.* **2005**, *38*, 317.
(22) Goldstein, S.; Samuni, A.; Hideg, K.; Merenyi, G. *J. Phys. Chem. A* **2006**, *110*, 3679.
(23) Grynova, G.; Barakat, J. M.; Blinco, J. P.; Bottle, S. E.; Coote, M. L. *Chem. Eur. J.* **2012**, *18*, 7582.
(24) Burks, S. R.; Makowsky, M. A.; Yaffe, Z. A.; Hoggle, C.; Tsai, P.; Muralidharan, S.; Bowman, M. K.; Kao, J. P. Y.; Rosen, G. M. *J. Org. Chem.* **2010**, *75*, 4737.
(25) Stoll, S.; Schweiger, A. *J. Magn. Reson.* **2006**, *178*, 42 (http://www.easyspin.org).
(26) Ysacco, C.; Karoui, H.; Casano, G.; Le Moigne, F.; Combes, S.; Rockenbauer, A.; Rosay, M.; Maas, W.; Ouari, O.; Tordo, P. *Appl. Magn. Reson.* **2012**, *43*, 251.
(27) Riplinger, C.; Kao, J. P. Y.; Rosen, G. M.; Kathirvelu, V.; Eaton, G. R.; Eaton, S. S.; Kutateladze, A.; Neese, F. *J. Am. Chem. Soc.* **2009**, *131*, 10092.
(28) Ottaviani, M. F.; Modelli, A.; Zeika, O.; Jockusch, S.; Moscatelli, A.; Turro, N. J. *J. Phys. Chem. A* **2012**, *116*, 174.
(29) Zeika, O.; Li, Y.; Jockusch, S.; Parkin, G.; Sattler, A.; Sattler, W.; Turro, N. J. *Org. Lett.* **2010**, *12*, 3696.
(30) Nogami, T.; Ishida, T.; Yasui, M.; Iwasaki, F.; Takeda, N.; Ishikawa, M.; Kawakami, T.; Yamaguchi, K. *Bull. Chem. Soc. Jpn.* **1996**, *69*, 1841.
(31) Spirk, S.; Belaj, F.; Madl, T.; Pietschnig, R. *Eur. J. Inorg. Chem.* **2010**, 289.
(32) Boča, R. *A Handbook of Magnetochemical Formulae*; Elsevier: Amsterdam, 2012.
(33) Kahn, O. *Molecular Magnetism*; VCH: New York, 1993.
(34) Bushmakina, N. G.; Misharin, A. Y. *Synthesis* **1986**, 966.
(35) Song, Y.-Z.; Zhou, J.-F.; Zhu, F.-X.; Ye, Y.; Xie, J.-M. *Comput. Biol. Med.* **2010**, *40*, 671.
(36) Duling, D. R. *J. Magn. Reson.* **1994**, *104*, 105 (http://www.niehs.nih.gov/research/resources/software/tox-pharm/tools/index.cfm).
(37) Becke, A. D. *J. Chem. Phys.* **1993**, *98*, 5648.
(38) Head-Gordon, M.; Head-Gordon, T. *Chem. Phys. Lett.* **1994**, *220*, 122.
(39) Woon, D. E.; Dunning, T. H., Jr. *J. Chem. Phys.* **1993**, *98*, 1358.
(40) Frisch, M. J.; Trucks, G. W.; Schlegel, H. B.; Scuseria, G. E.; Robb, M. A.; Cheeseman, J. R.; Scalmani, G.; Barone, V.; Mennucci, B.; Petersson, G. A.; Nakatsuji, H.; Caricato, M.; Li, X.;Hratchian, H. P.; Izmaylov, A. F.; Bloino, J.; Zheng, G.; Sonnenberg, J. L.; Hada, M.;

Ehara, M.;Toyota, K.; Fukuda, R.; Hasegawa, J.; Ishida, M.; Nakajima, T.; Honda, Y.; Kitao, O.; Nakai, H.;Vreven, T.; Montgomery, J. A., Jr.; Peralta, J. E.; Ogliaro, F.; Bearpark, M.; Heyd, J. J.; Brothers, E.; Kudin, K. N.; Staroverov, V. N.; Kobayashi, R.; Normand, J.; Raghavachari, K.; Rendell, A.; Burant, J. C.; Iyengar, S. S.; Tomasi, J.; Cossi, M.; Rega, N.; Millam, N. J.; Klene, M.; Knox, J. E.; Cross, J. B.; Bakken, V.; Adamo, C.; Jaramillo, J.; Gomperts, R.; Stratmann, R. E.; Yazyev, O.; Austin, A. J.; Cammi, R.; Pomelli, C.; Ochterski, J. W.; Martin, R. L.; Morokuma, K.; Zakrzewski, V. G.; Voth, G. A.; Salvador, P.; Dannenberg, J. J.; Dapprich, S.; Daniels, A. D.; Farkas, Ö.; Foresman, J. B.; Ortiz, J. V.; Cioslowski, J.; Fox, D. J. *Gaussian 09, Revision A.1*; Gaussian, Inc., Wallingford, CT, 2009.

(41) Barone, V.; Cossi, M. *J. Phys. Chem. A* **1998**, *102*, 1995.

(42) Barone, V. *Chem. Phys. Lett.* **1996**, *262*, 201.

(43) Rega, N.; Cossi, M.; Barone, V. *J. Chem. Phys.* **1996**, *105*, 11060.

(44) Fritscher, J.; Beyer, M.; Schiemann, O. *Chem. Phys. Lett.* **2002**, *364*, 393.

(45) *CrysAlisPro, Version 1.171.36.20*; Oxford Diffraction Ltd., Abingdon, Oxford, England, 2012.

(46) Sheldrick, G. M. *Acta Crystallogr.* **2008**, *A64*, 112.

(47) Brandenburg, K. Berndt, M. *DIAMOND*; Crystal Impact GmbH, Bonn, Germany, 1999.